JOURNAL OF MATERIALS SCIENCE 19 (1984) 2246–2258

Effect of temperature and strain rate on the strength of a PET/glass fibre composite

J. M. SCHULTZ,* K. FRIEDRICH†
Institute für Werkstoffe, Ruhr-Universität Bochum, 4630 Bochum, West Germany

Constant strain-rate mechanical testing and surface fractography were used to characterize the failure behaviour of a PET/glass injection-moulding compound and of its unfilled matrix material. Parameters for this investigation were temperature and strain rate. The matrix material exhibited a viscous–brittle transition between room temperature and 60° C. Low temperature failure occurred by craze growth, followed by slow and rapid crack propagation. The composite material likewise behaved as a viscous solid at superambient temperatures. Failure at low temperatures and/or high deformation rates occurred by brittle matrix fracture and fibre pull-out. Under these conditions, mechanical properties improved, relative to those at room temperatures. At intermediate temperatures and/or low strain rates, failure occurred via matrix crazing and crack propagation near the fibre ends. An observed serration of the fracture path at high strain rates is suggested to be due to the need for high shear stresses at the fibre–matrix interface.

1. Introduction

The utilization of short-fibre/polymer composites in increasingly more stringent mechanical conditions dictates that the failure behaviour of such materials be well documented and understood. Increasingly more attention is, therefore, being paid to the fracture [1–4], fatigue [1, 3, 4–10], stress rupture [9, 11–13] and stress-corrosion [11–19] of short-fibre systems. Depending upon the specific composite and on the loading conditions, the crack path has been observed to proceed around the fibre/matrix interface (debonding), through the matrix (fibre-avoidance), or through the fibres. It is still not sufficiently clear under precisely what conditions each of the above paths obtains, what the influence of matrix behaviour is, or how the crack propagation characteristics influence the macroscopic behaviour. The present work represents a step in the direction of the characterization of propagation modes and their transitions, as influenced by temperature and deformation rate for a specific composite material and its unreinforced thermoplastic matrix. The work was undertaken and is presented in the spirit of identification of dominant fracture mechanisms and their effects on the work of fracture, the tensile strength, and the modulus.

2. Experimental details

The composite used was Rynite^{R} 530, a modified poly(ethylene terephthalate) (PET) resin, reinforced with approximately 30 wt% chopped E-glass fibres. The matrix itself possesses a two-phase microstructure, consisting of discrete rubbery particles dispersed in the PET continuum [20]. Both the composite material and the unfilled resin were supplied by E. I. Du Pont de Nemours, Inc., in the form of end-gated injection-moulded plaques. The dimensions of the plaques are 125 mm x 76.2 mm x 3.2 mm. The microstructure across the thickness of a composite plaque is strongly inhomogeneous and anisotropic. To a depth of about 1.2 mm from either broad

*On leave from the Center for Composite Materials and Department of Chemical Engineering, University of Delaware, Newark, Delaware 19711, USA.
†Present address: Arbeitsbereich Kunststoffverarbeitung, Technische Universität Hamburg-Harburg, 2000 Hamburg 90, West Germany.

0022–2461/84 $03.00 + .12

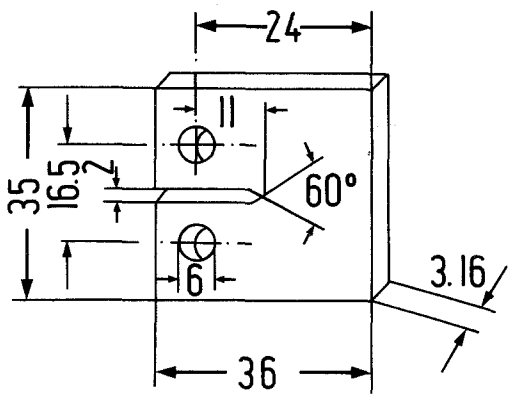

Figure 1 Dimensions (mm) of compact tension specimens used throughout this work.

surface, the fibres are strongly aligned parallel to the mould-fill direction (MFD) [10, 11, 12, 21]. The fibres in the remaining core (~ 0.8 mm) are oriented in the plane of the plaque and perpendicular to the MFD. Within the matrix, the lamellar PET crystallites are aligned with their thin dimension approximately perpendicular to the fibres [22], an effect apparently deriving from the differential thermal contractions of polymer and glass during crystallization.

Compact tension (CT) specimens with the geometry shown in Fig. 1 were used throughout the present work. For both the composite material and the unfilled resin, the tensile axis was parallel to the MFD. In the case of the composite, then, over approximately three-quarters of the cross-section the fibres lie across the crack paths; only in the core is there a path of easy propagation.

Mechanical testing was performed using a Zwick mechanical tester. Strain rates varied between 0.005 and 500 mm min^{-1}. From 0.005 to 50 mm min^{-1}, a strip-chart recorder was used to record the force–deflection data. Beyond 50 mm min^{-1}, a digital oscilloscope was used, because the mechanical inertia of the strip-chart pen caused it to lag. Temperatures used were -80, $-20°$ C, room temperature (25° C), 60 and 120° C.

Optical microscopy was performed using a low power stereomicroscope. Scanning electron microscopy (SEM) was carried out using several available instruments. Fracture surfaces were gold-sputtered prior to SEM observation.

3. Results

3.1. Mechanical behaviour

For both matrix resin and composite a much greater sensitivity to temperature than to strain rate was observed. Figs. 2 and 3 show the change in the force–displacement curves for both materials at a given, arbitrary strain rate (5 mm min^{-1}). The matrix material shows brittle behaviour from $-80°$ C to room temperature. At 60° C, a reduction in initial modulus and the onset of plastic behaviour are observed. These tendencies are amplified at 120° C. The change in behaviour at

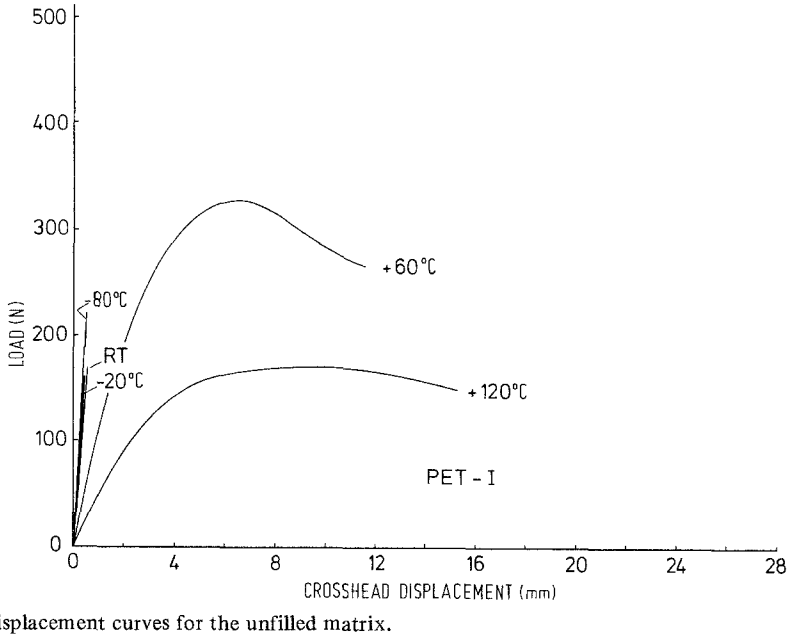

Figure 2 Load–displacement curves for the unfilled matrix.

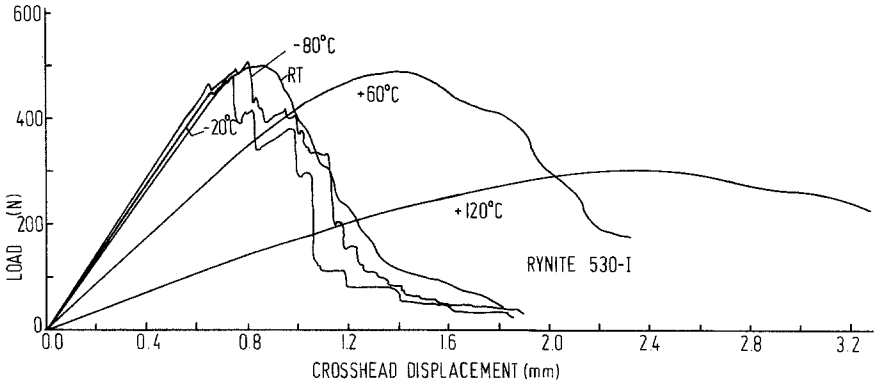

Figure 3 Load–displacement curves for the PET/glass composite.

60° C is expected, as PETs generally exhibit a glass transition near this temperature. At the two higher temperatures considerable plastic flow occurred at the root of the notch and no specimens fractured completely through the section. For the composite, serrated force–displacement curves are seen at the two lower temperatures. That is, regions of increasing crosshead displacement with little change in load are followed by sudden drops in the load. At room temperature (approximately 25° C), these easy deformation and load drop transitions are smoothed out. As the temperature is further increased, the modulus decreases and the load–displacement curves become smoother.

The following properties were read from the load–displacement curves: initial slope (N cm^{-1}), maximum load (N), and the work to achieve the maximum load (N cm). In order to demonstrate relative changes and to relate to more fundamental parameters, these values are normalized by dividing by the same parameter from "standard" specimens. Chosen for the matrix and composite standards were specimens deformed at 5 mm min^{-1} at room temperature. Since the initial slope is directly proportional to the tensile modulus, the normalized slope E^* represents the ratio of moduli between a given specimen and the standard. In the same way, the normalized work to attain the load maximum, W^*, is the "work of failure initiation" ratio between the given specimen and the standard, and the normalized maximum load σ_T^* is loosely related to the ratio of tensile strengths.

Fig. 4 shows the changes of normalized modulus, work of failure, and ultimate stress with temperature and deformation rate for the matrix material. Probably the most striking features are the strength maximum at 60° C and the tendency of the room temperature properties to change with decreasing deformation rate toward those observed at the higher temperatures.

The effects of strain rate and temperature on

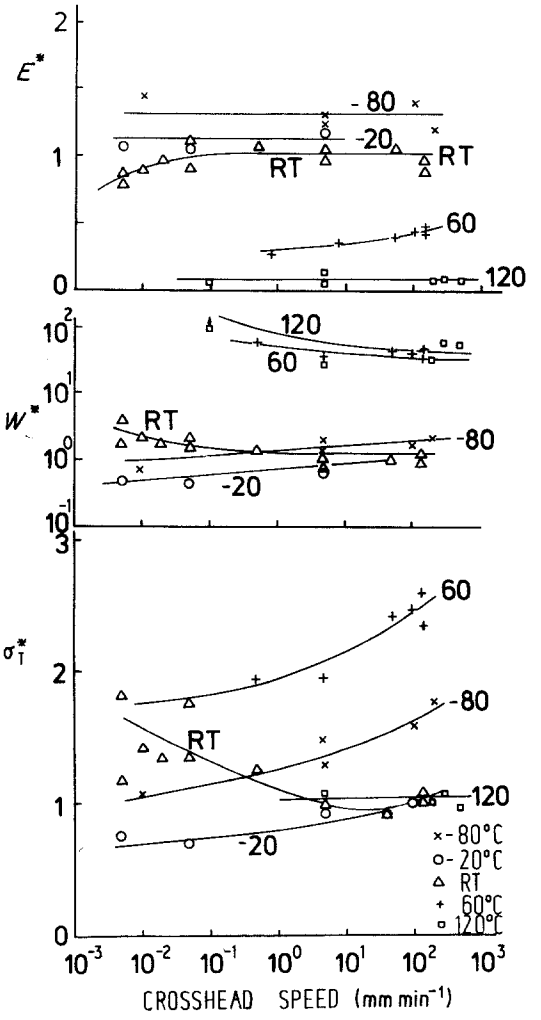

Figure 4 Normalized mechanical properties for the unfilled matrix material.

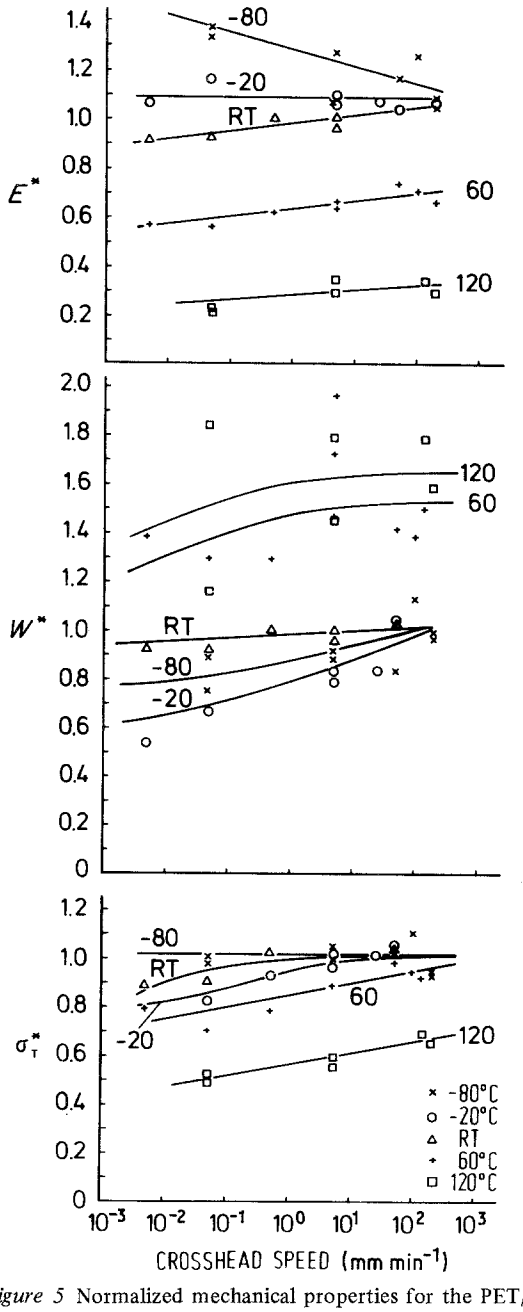

Figure 5 Normalized mechanical properties for the PET/glass composite.

the mechanical behaviour of the composite are shown in Fig. 5. The expected drops in modulus and tensile stress as the matrix goes through its glass transition are evident. The greater matrix ductility is reflected also in a large increase in the work of failure. The most surprising effect, however, is that the ultimate stress and work of failure are both slightly higher at $-80°$ C than at $-20°$ C. This inversion will be treated later. Finally, the values of all properties at almost all temperatures increase with deformation rate. Similar increases in E^* and W^* are not observed for the unfilled material. The strain rate effect thus appears to reflect the incorporation of fibres.

In order to explicitly see the effect of fibres on the strength of the material, one can relate all values of strength to that of the matrix at the standard condition (RT, 5 mm min^{-1}). Fig. 6 shows this normalized strength, $\bar{\sigma}_T^{**}$, plotted against temperature, for extremes of deformation rate. Two effects are especially to be noted. First, a principal effect of the fibres is to maintain a high strength at low temperatures, even while the matrix becomes embrittled. Second, the peak in matrix strength moves toward higher temperatures at higher deformation rates. It should also be noted that above 60° C, the curves for unfilled and filled material approach each other.

For the composite, the modulus and the tensile strength are correlated. The correlation is shown in Fig. 7. This parallelism enables one to measure either σ_T^* or E^* and reliably infer the other parameter.

It is useful to map the behaviour of the composite in a single graph [23, 24] from which engineering decisions can be made. One such mapping is shown in Fig. 8. This map shows values of modulus plotted against work of failure. (Note that a map of tensile strength against work would show similar features.) In the map, solid lines represent isodeformation-rate contours and dashed lines represent isothermal contours. The map region lying, for instance, above $E^* = 0.8$ represents all conditions for which the modulus is at least 80% that of the standard. The region lying to the right of $W^* = 0.8$ contains all conditions for which the work of failure is at least 80% of that of the standard. The right angle marked 80% contains, therefore, all conditions under which both E^* and W^* are at least 80% of the standard. If engineering usage requires that both E^* and W^* lie above 80% (for instance), then the material is restricted to either (a) room temperature or very low temperature ($-80°$ C and below) use at all strain rates, or (b) to RT and any lower temperatures, providing that slow or continuous loading can be avoided. Two elements of behaviour seen in Fig. 8 will be discussed in detail below. These are in the inversion in

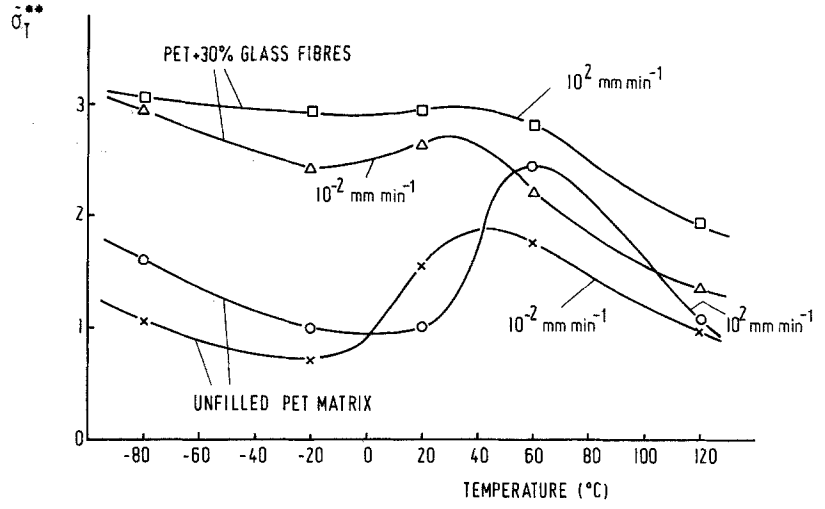

Figure 6 Average normalized tensile strength $\bar{\sigma}_T^{**}$ (related to strength of unfilled matrix at RT and 5 mm min^{-1}).

behaviour from -20 to $-80°$ C and the general maintenance of good properties at low temperatures, despite matrix embrittlement.

3.2. Fractography

Both the macroscopic course of the fracture path and the details of the fracture surface change with deformation rate and temperature. Fig. 9 shows fracture paths for slowly and rapidly deformed matrix specimens at each temperature. Above room temperature, the material at the crack tip thins and pulls apart in a viscous manner. Below room temperature, the materials show nearly featureless, flat paths and appear perfectly brittle. In fact, as will be shown, crazes form in the early stages, even for these failures. At room temperature, two types of behaviour have been seen at the lowest deformation rate used, 0.005 mm min^{-1}. One specimen behaved brittly and the other in a viscous manner. In agreement with the mechanical results, very low strain rates at room temperature can produce viscous behaviour.

Fig. 10 illustrates the fracture path tendencies for the composite, from low to high temperatures and high to low deformation rates. At room temperature and below, the fracture path tends to become macroscopically more jagged as one progresses from high to low temperature or from low to high deformation rate. The edges of the zig-zag lie at approximately 45° to the tensile

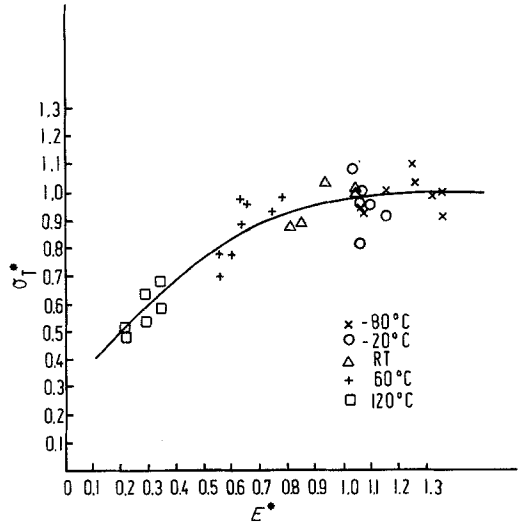

Figure 7 Normalized tensile stress plotted against normalized modulus for the PET/glass composite.

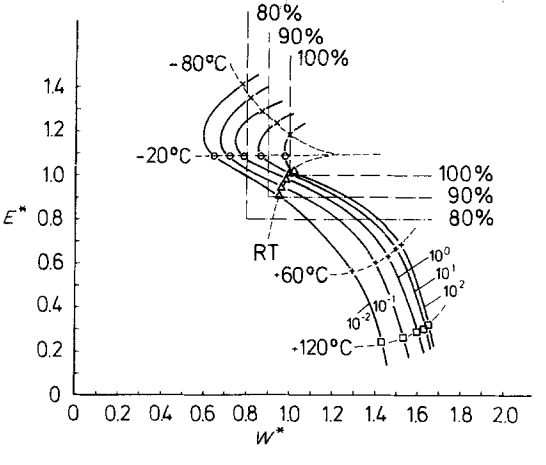

Figure 8 Mechanical behaviour map for the PET/glass composite.

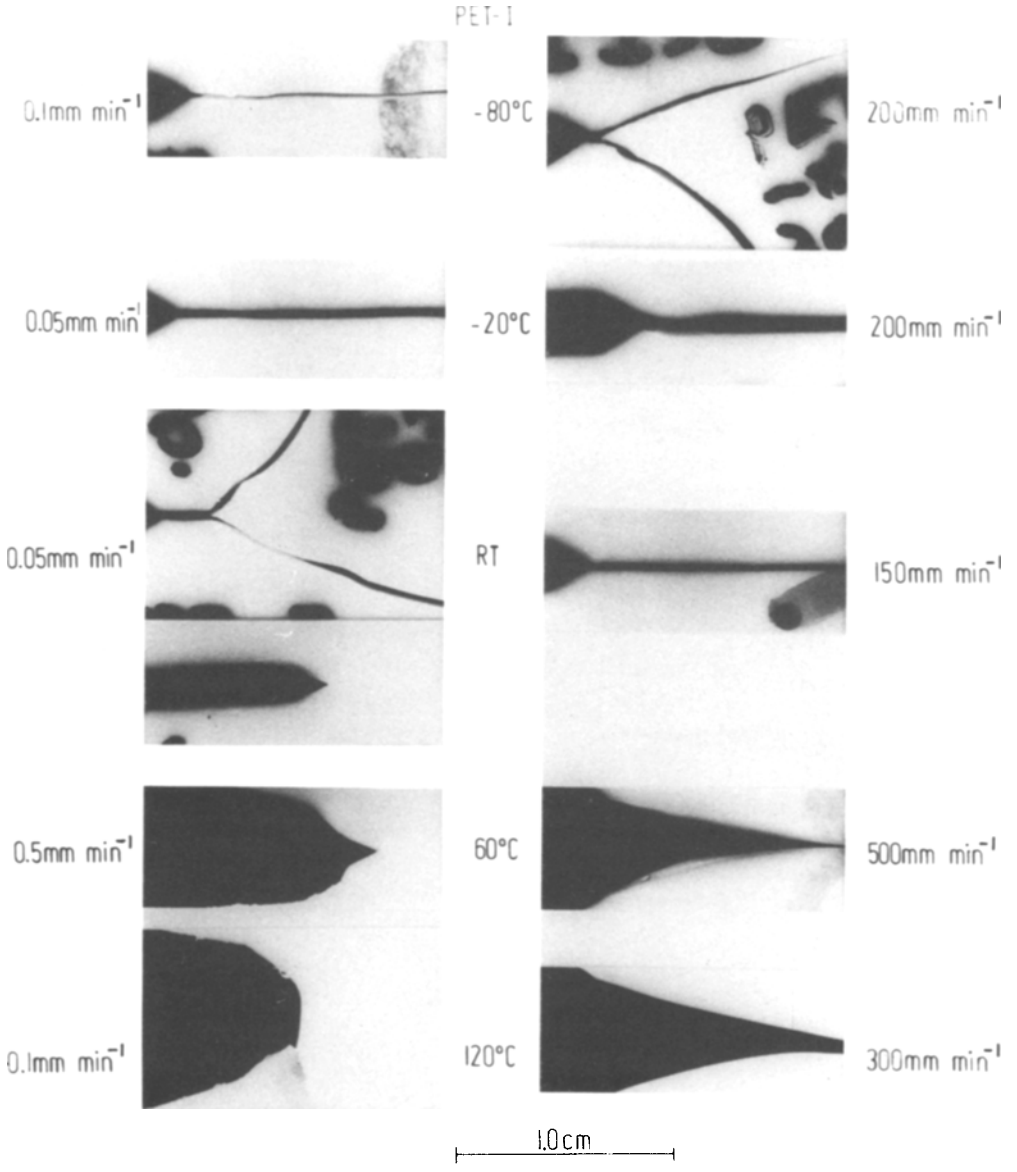

Figure 9 Optical micrographs of the fracture path for the unfilled matrix material. Original notch seen at the left in each micrograph. Note that at RT and 0.005 mm min^{-1} the matrix has exhibited both brittle (upper micrograph) and viscous (lower micrograph) behaviour.

axis. At the higher temperatures (60 and 120° C), the fracture path is independent of deformation rate. In this case, the path is a fine zig-zag, with stress-whitened edges. In the original micrographs, it can be seen that the saw-tooth patterns always are associated with the pull-out of lengths of fibre, whereas the smoothest paths are associated with the pull-out of only short lengths of fibre.

Selected low magnification scanning electron micrographs of areas near the notch (seen as a smooth, slanted region at the lower left corner of each micrograph) are shown in Fig. 11. Below the glass transition (Fig. 11a), the first stage of fracture is the creation of a craze at the notch tip (arrow) and the propagation of a crack through this craze. Above the glass transition (Fig. 11b) no initiation zone is seen, only a massive viscous flow. Even at the lowest temperature studied, −80° C, such an initial craze zone is created (arrow on Fig. 12a). Most crazes propagate only a few tens of a millimetre before unstable crack propagation occurs. Most likely, in these cases, crazes act only to provide a crack with small tip radius. Only under extremely slow crack

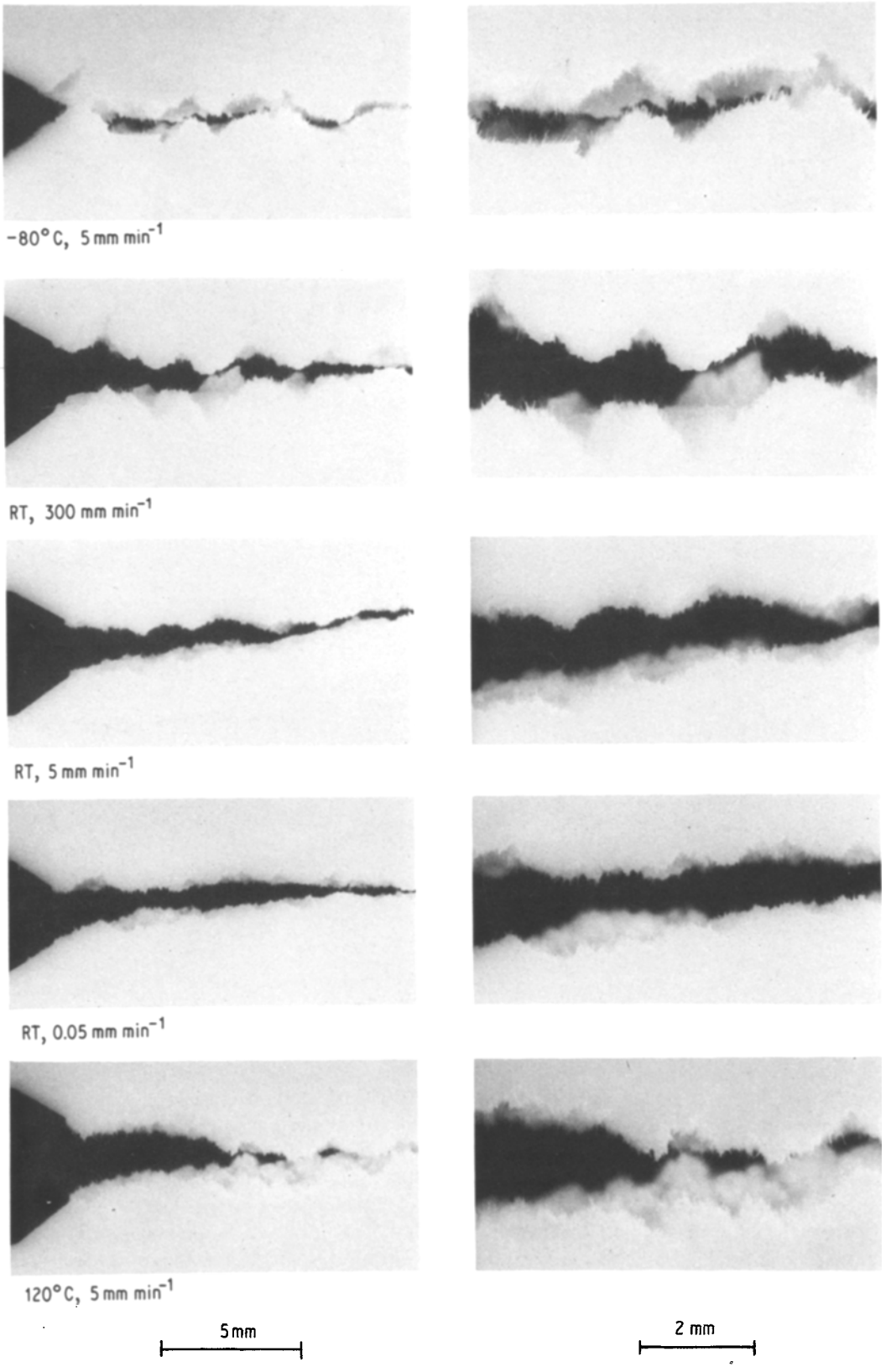

Figure 10 Optical micrographs of the PET/glass composite. Original notch seen at the left in each micrograph.

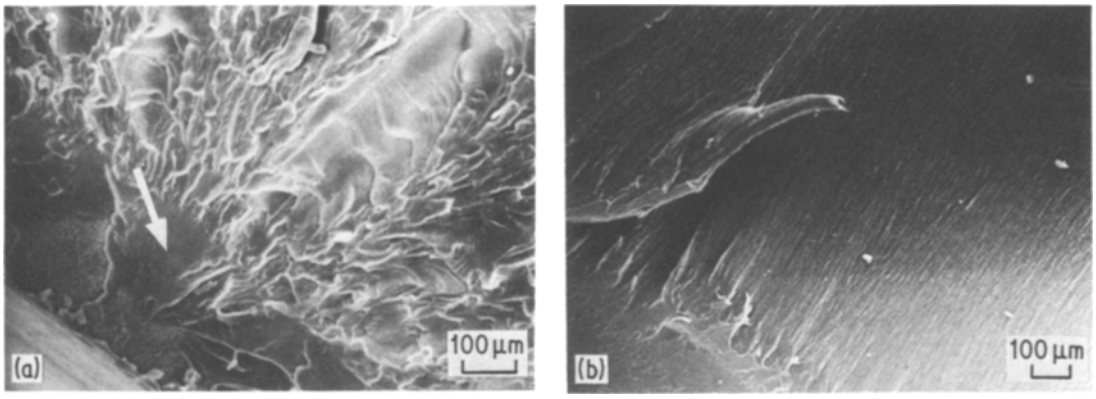

Figure 11 Selected low magnification SEM micrographs of unfilled matrix fracture surfaces: (a) — 80° C, 5 mm min^{-1}; (b) 120° C, 300 mm min^{-1}.

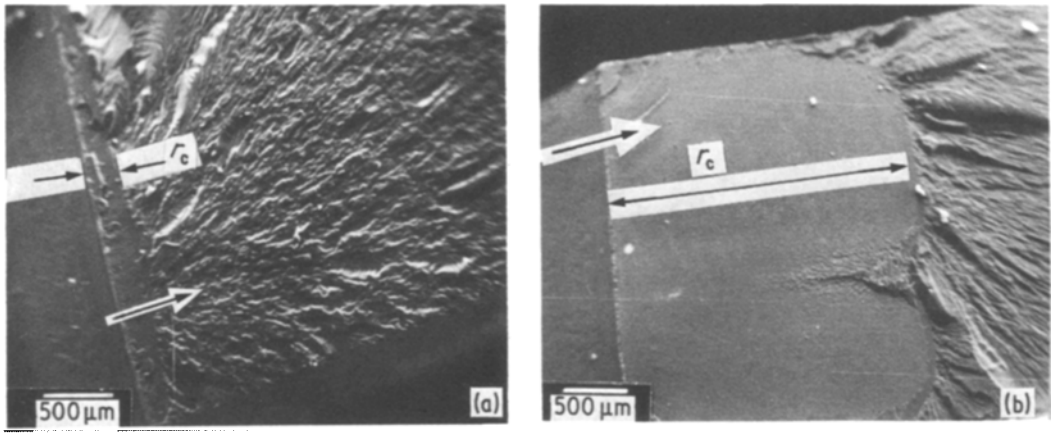

Figure 12 Size of initial craze zone, r_c, on the fracture surface of PET-matrix material as a function of testing temperature: (a) — 80° C, 0.01 mm min^{-1}, $r_c \approx 250$ µm; (b) — 20° C, 0.005 mm min^{-1}, $r_c \approx 2.5$ mm. The arrow indicates the direction of craze and crack propagation.

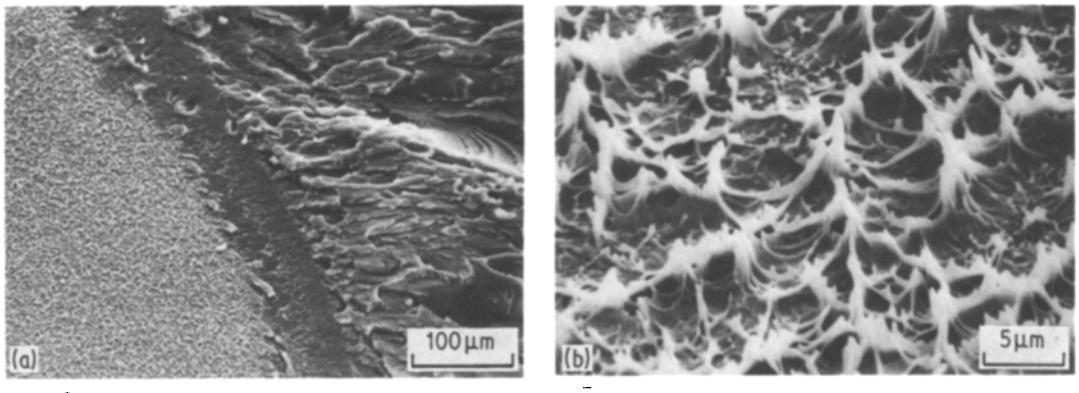

Figure 13 Higher magnification scanning electron micrographs of the unfilled matrix, deformed at — 20° C, 0.05 mm min^{-1}: (a) transition from crazed region to brittle fracture; (b) ruptured fibrillar craze texture.

opening conditions (-0.05 mm min^{-1}) in the temperature range between $-20°$ C and RT longer extensions of the crazed area, i.e. the region of stable crack growth were observed (Fig. 12b).

Selected higher magnification scanning electron micrographs shown in Fig. 13 represent, for slow displacement rate failure at $-20°$ C, the transition from initial craze fracture to brittle fracture (from left to right on Fig. 13a). What is especially to be noted is that the broken craze texture consisting of tip-like polymer bundles coarsens as the temperature of deformation increases. Indeed, the viscous flow thinning can be thought of as the limit of very coarse crazing. The fineness of the craze detail reflects the viscosity of the mater-

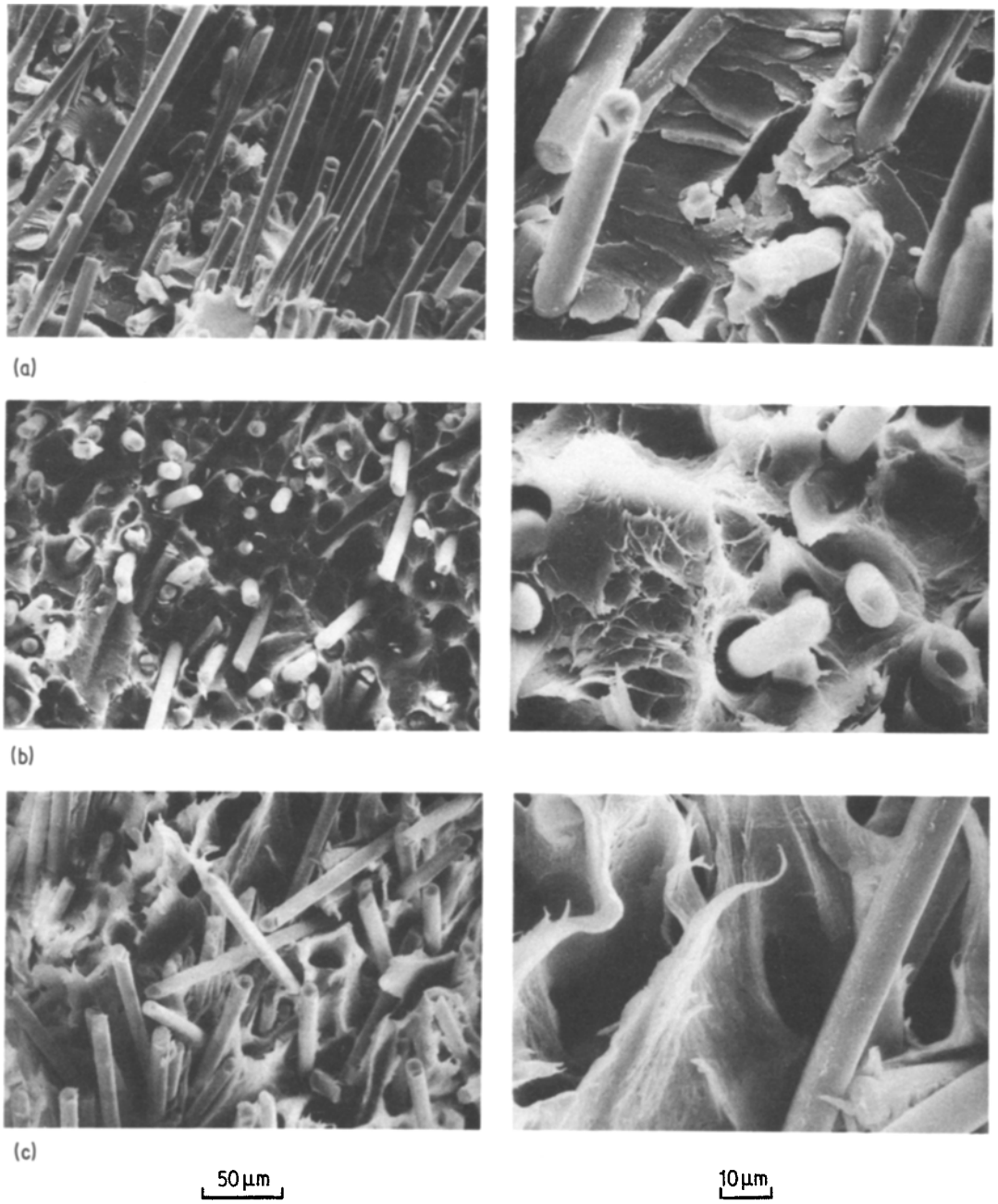

Figure 14 Scanning electron micrographs of failure surfaces of the composite at (a) $-80°$ C, 5 mm min^{-1}; (b) RT, 5 mm min^{-1}; and (c) 120° C, 5 mm min^{-1}.

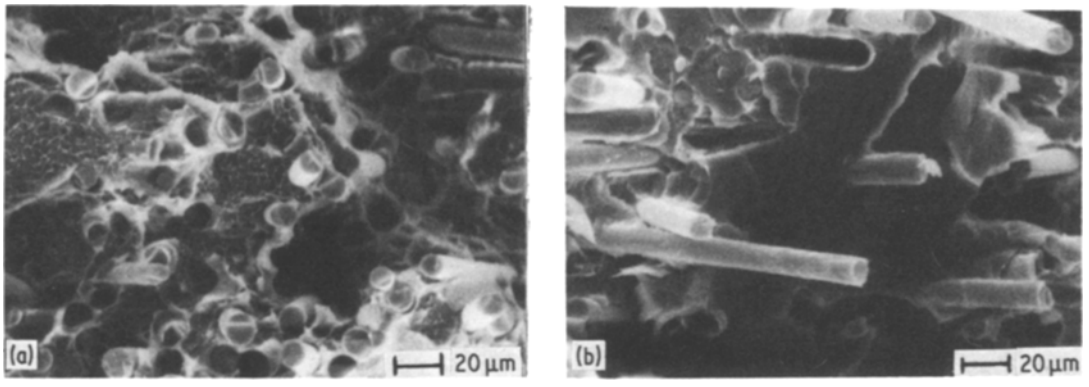

Figure 15 Scanning electron micrographs of failure surfaces of the composite at $-20°$ C, 0.005 mm min^{-1} : (a) near the notch, (b) far from notch.

ial, fine crazes indicating a flow instability at high viscosity.

The fractography of the composite is illustrated in Figs. 14 and 15. Fig. 14 shows micrographs taken from the regions near the notch and typical of low temperature, room temperature and high temperature, respectively. At low temperatures and medium or high strain rates (Fig. 14a), fibres pull smoothly out of the matrix while the matrix fractures in a brittle manner. A similar fracture pattern is also found in the regions of rapid crack propagation (far away from notch) of specimens broken at room temperature or below. Near and above the glass transition, viscous matrix flow and fibre pull-out constitute the failure processes (Fig. 14c).

The behaviour at room temperature is, however, different from either high or low temperature failure. In Fig. 14b we see that specimen separation occurs mostly at fibre tips or through

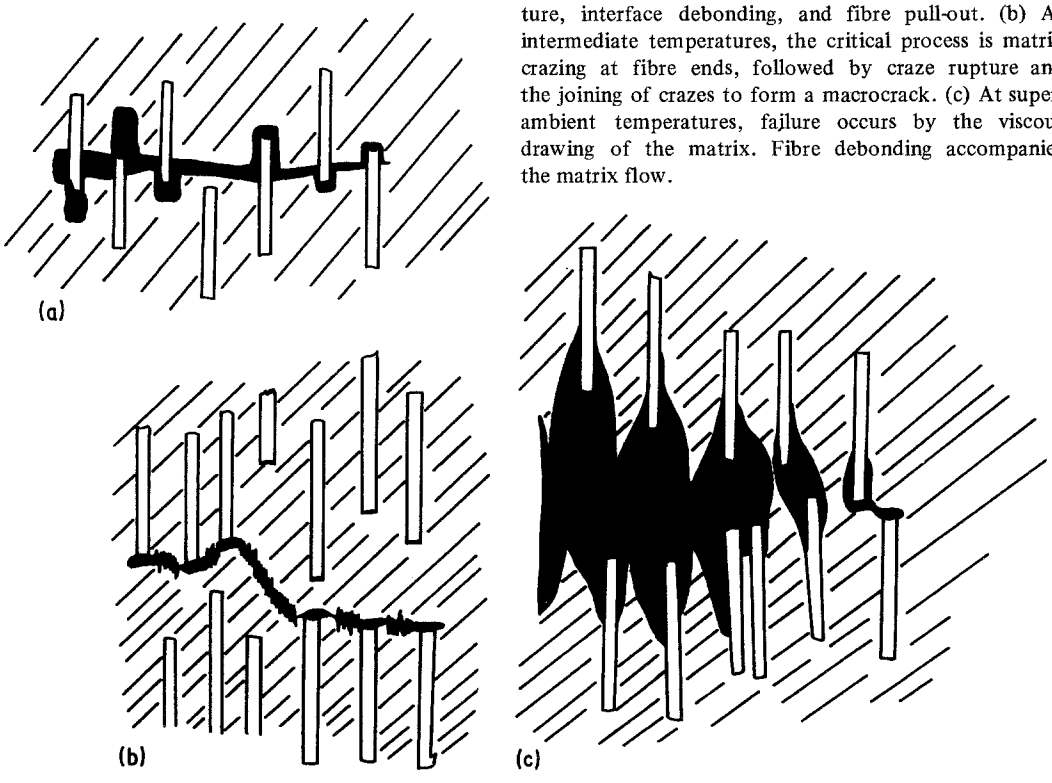

Figure 16 Sketch of modes of failure in PET/glass composite. (a) At subambient temperatures or RT and rapid deformation rates, failure occurs by matrix brittle fracture, interface debonding, and fibre pull-out. (b) At intermediate temperatures, the critical process is matrix crazing at fibre ends, followed by craze rupture and the joining of crazes to form a macrocrack. (c) At superambient temperatures, failure occurs by the viscous drawing of the matrix. Fibre debonding accompanies the matrix flow.

broken fibres (with occasional pull-out of short fibre ends) after a craze or viscous-like failure of the polymer matrix in between. Similar fracture behaviour has been previously associated with high cycle fatigue failure [8, 10] at room temperature and with stress rupture under low loads [9]. Crack propagation along fibre tips is also found for slow deformation rate and -20° C (Fig. 15a), for which, in addition, the crazing mechanism of the matrix is more pronounced. This behaviour is analogous to that of the unfilled resin under comparable conditions (see Fig. 13b), except that for the composite the local stress is raised additionally at the fibre tips. Further from the notch, the cracks propagate by fibre pull-out and brittle matrix fracture (Fig. 15b).

For the composite, three different modes of failure in the crucial region near the notch have been observed. These are now schematically illustrated in Fig. 16. At low temperatures and sufficiently high deformation rates, fibre debonding and pull-out are accompanied by brittle matrix failure. At intermediate temperatures and sufficiently low strain rates, matrix cracks propagate through crazes formed at fibre tips. This process obviates the need for fibre/matrix debonding and pull-out, but requires time for craze formation. At higher temperatures, the matrix fails in a viscous manner, accompanied by fibre debonding. In this case, the matrix viscosity appeared to be insufficient to transfer load well between fibres. Debonding occurs only as the fibres offer geometrical constraints to the flow of the matrix. Examination of numerous fracture surfaces has lead to the failure behaviour map of Fig. 17.

4. Discussion

The discussion centres on three phenomena: the retention, and even improvement, of strength and work of failure of the composite at low temperature, the minima in properties at some -20° C and low strain rate, and the causes of the serrated fracture path at high strain rates or low temperatures.

The excellent low temperature behaviour reflects the relative temperature independence of the chief mode of low temperature energy absorption: fibre pull-out. Previous work on this material at room temperature [10] has already quantitatively defined this as the chief energy absorbing failure mechanism and the present investigation indicates that fibre pull-out is still dominant at -80° C. This is a friction-like action and should have relatively little temperature dependence, provided that fibre and matrix contact remains geometrically similar. It is possible even that the differential fibre/matrix thermal contraction would promote greater frictional force as the temperature is lowered, thereby increasing the ultimate strength and the work of failure. At any event, the possible use of short-fibre composites as low temperature mechanical protection devices or armour is indicated.

The relatively low work of fracture found at -20° C and low strain rates is attributed to short-circuiting of the fibre pull-out mode. In this case, the short-circuiting was achieved via time-dependent crazing and fracture in the stress-enhanced regions at fibre ends. This type of failure has been previously observed in short-fibre composites [2, 6, 9–11] and appears to be a characteristic of time-dependent failure at low stresses [9–11].

The deeply serrated fracture paths at high deformation rates is puzzling. At first thought, one would be tempted to associate such behaviour with the joining of microcracks formed in front of the main crack tip. Indeed, rugged fracture paths do arise from such sources [9–11] and a statistical theory of crack joining has been developed [25, 26]. However, such behaviour should be most severe at higher temperatures and lower strain rates, where the required time-dependent matrix plasticity (shear or crazing) can develop. Just the opposite is observed here.

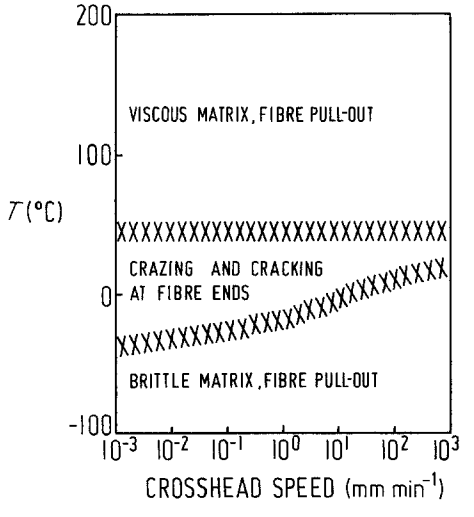

Figure 17 Failure behaviour map for PET/glass composite.

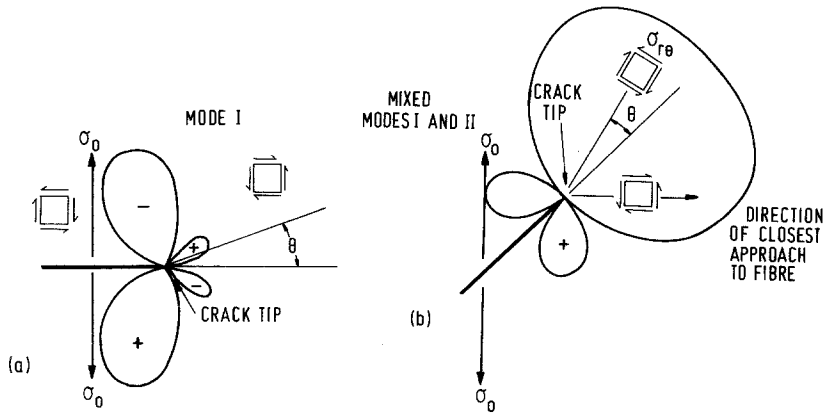

Figure 18 Shear stress fields about crack tip: (a) σ_{XY} shear stress about a pure Mode I crack, at 90° to the tensile direction; (b) $\sigma_{r\theta}$ shear stress about a mixed Mode I/Mode II crack at 45° to the tensile direction.

In fact, conditions of matrix plasticity enhance fibre-end fracture and produce a fracture path more nearly perpendicular to the applied load.

A more likely explanation is rooted in the nature of fibre–matrix debonding and pull-out. Both of these processes operate from shear, not normal, stresses, and the debonding should show some time or temperature dependence. Since these principal failure processes require shear stresses, they will be enhanced by crack geometries which produce large shear stresses. Fig. 18a shows the shear stress ahead of a Mode I crack propagating normal to the applied load [27]. If such a crack inclines away from the plane normal to the applied stress, then mixed Mode I and Mode II behaviour ensues. Mode II is essentially a shear process and results in increased shear stress near the crack tip. Fig. 18b shows the radial shear stress field about a mixed mode crack inclined at 45° to the tension. Such a crack propagating through the matrix will produce a much higher shear stress at the interface than will a Mode I crack. At relatively low strain rates, time-dependent creep and rupture can occur at the interface. In this case, the interface can debond and fibres can pull out at relatively low stresses and Mode I cracking should suffice. At higher deformation rates, the kinetics of debonding and pull-out can demand the higher interfacial shears which are supplied by the mixed mode crack. The directional changes of the zig-zag path are somewhat less easily explained, but likely result from the need for a crack to optimize its own propagation conditions by shifting locally toward Mode I behaviour [27]. Presumably, such path shifting occurs when either (a) a fibre-poor zone is encountered, or (b) local average fibre orientations are unfavourable for shear rupture at the interface. Once the crack has become normal to the tensile stress it can seek a new path inclined at either a large positive or negative angle.

5. Conclusion

The matrix material exhibits plastic (viscous) behaviour at superambient temperatures. At room temperature and below, failure occurs by the creation of a craze, followed by through-craze slow crack propagation and, finally, by unstable crack propagation. The strain-rate sensitivity is not great, although at room temperature the material behaviour changes at very low rates from brittle to ductile.

The PET/glass composite exhibits serrated force–deflection curves and serrated crack propagation paths. The ultimate properties improve at low temperatures, although a valley in performance is seen at approximately $-20°$ C for lower deformation rates. This valley is attributed to the initiation of crazes – and subsequently cracks – at fibre ends, a mechanism which obviates fibre pull-out. Fibre pull-out is observed at the lowest temperatures and/or at higher deformation rates and is associated with high failure energies. The serrated fracture surfaces are likely the result of the requirement of high shear stresses at fibre interfaces.

Acknowledgement

The authors gratefully acknowledge the help of Mr K. -H. Bowe, without whose expertise the mechanical testing programme would have found-

ered, and Professor E. Hornbogen, who provided very useful discussions and encouragement and with those facilities the work was carried out. This work was supported by the Alexander von Humboldt-Stiftung and the Heinrich-Hertz-Stiftung.

References

1. S. GAGGAR and L. BROUTMAN, ASTM STP 631 (American Society for Testing and Materials, Philadelphia, 1977) p. 310.
2. P. T. CURTIS, M. G. BADER and T. F. BAILEY, *J. Mater. Sci.* **13** (1978) 377.
3. K. FRIEDRICH, *Coll. Polymer Sci.* **259** (1981) 808.
4. *Idem, Kunststoffe* **72** (1982) 290.
5. F. J. MCGARRY, E. H. ROW and C. K. RIEW, *Polymer Eng. Sci.* **18** (1978) 78.
6. R. A. HEIMBUCH and B. A. SANDERS, "Mechanical Properties of Automotive Chopped Fiber Reinforced Plastics" (General Motors Corporation Manufacturing Development, G.M. Technical Center, Warren, Michigan, 1978).
7. J. F. MANDELL, *Polymer Composites* **2** (1981) 22.
8. MILDRED R. JEFFERY, JANINE A. SOUROUR and J. M. SCHULTZ, *ibid.* **3** (1982) 18.
9. C. LHYMN and J. M. SCHULTZ, *J. Mater. Sci.* **18** (1983) 2029.
10. JEAN C. MALZAHN, MChE thesis, University of Delaware (1983).
11. K. FRIEDRICH, *J. Mater. Sci.* **16** (1981) 3292.
12. *Idem, Prakt. Metallogr.* **18** (1981) 513.
13. *Idem, Plastverarbeiter* **33** (1982) 47.
14. R. C. ALLEN, *Polymer Eng. Sci.* **19** (1979) 329.
15. D. HULL and P. J. HOGG, "Proceedings 3rd International Conference on Composite Materials", Paris, Vol. 1 (Pergamon Press, Oxford 1980) p. 543.
16. J. AVESTON, *ibid.* p. 556.
17. W. S. CARSWELL and R. C. ROBERTS, *Composites* **11** (1980) 95.
18. C. LHYMN and J. M. SCHULTZ, *J. Mater. Sci.* **18** (1983) 2923.
19. *Idem, Polymer Sci. Eng.*, to be published.
20. I. WITTKAMP, K.-H. BOWE and K. FRIEDRICH, *Beitr. elektronenmikroskop. Direktabb. Oberfl.* **15** (1982) 245.
21. R. C. WETHERHOLD, W. A. DICK and R. B. PIPES, SAE Tech. Paper No. 800812 (1980).
22. C. LHYMN and J. M. SCHULTZ, *Polymer Composites*, to be published.
23. J. K. WELLS and P. W. R. BEAUMONT, *J. Mater. Sci.* **17** (1982) 397.
24. P. W. R. BEAUMONT, J. K. WELLS and P. D. ANSTICE, Proceedings 37th Annual Conference, Reinforced Plastics/Composites Institute, The Society of Plastics Industry (1982) Session 20-A.
25. M. G. BADER, T. W. CHOU and J. QUIGLEY, in "New Developments and Applications in Composites", edited by D. Wilsdorf (The Metallurgical Society, AIME, New York, 1979).
26. H. FUKUDA and T. W. CHOU, *J. Mater. Sci.* **16** (1981) 1088.
27. G. C. SIH (ed.), "Mechanics of Fracture", Vol. 1 (Noordhoff, Leyden, 1973).

Received 22 September
and accepted 4 October 1983